Numerical Simulation of Underground Coal Gasification Using the CRIP Method

Mojtaba Seifi, Zhangxin Chen and Jalal Abedi*

Department of Chemical & Petroleum Engineering, University of Calgary, Calgary, Alberta, Canada T2N 1N4

A three-dimensional simulation of the Underground coal gasification (UCG) process is studied in terms of the heat and mass transport phenomena and chemical kinetics in a coal seam during coal combustion by applying the controlled retracting injection point technique. The STARS module of the Computer Modelling Group software is used in this study. The gas species flow rate, cavity shapes, and temperature profile in the coal seam during gasification are investigated. The main motivation behind this study is to provide a simulation methodology by using a comprehensive porous media flow approach to understand the critical aspects of the UCG process.

Une simulation tridimensionnelle du processus de gazéification in situ du charbon (UCG) est étudiée en fonction de la chaleur, des phénomènes de transport de la matière ainsi que de la cinétique chimique dans une veine de charbon lors de sa combustion en appliquant la technique de rétraction contrôlée du point d'injection. Le module STARS du logiciel informatique de modélisation du groupe est utilisé dans cette étude. Le débit de l'espèce de gaz, les formes de cavités, et profil de température dans la veine de charbon lors de la gazéification sont étudiés. La principale motivation de cette étude est de fournir une méthodologie de simulation en utilisant une approche globale de l'écoulement en milieu poreux afin de comprendre les aspects critiques du processus de UCG.

Keywords: underground coal gasification, CRIP, pyrolysis, cavity, chemical reaction kinetics

INTRODUCTION

Coal as one of the fossil fuels currently provides 25% of the total energy demand of the world. It is being used either directly as a fuel in the furnaces or being gasified to a mixture of flammable gases that are mostly composed of H_2, CO, CH_4, CO_2, and slightly of H_2O, N_2, and H_2S. The product gas can be used either as a fuel for power generation or a chemical feedstock for various chemical products (e.g., hydrogen and ammonia; Perkins, 2005).

Most current technologies of coal gasification such as entrained flow, fluidised bed, and moving bed use a surface reactor for gasification. The main differences between these technologies relate to the gas flow configuration, coal particle size, ash handling, and process conditions. An alternative for surface gasifier is an underground coal gasifier that eliminates the need for mining and can be used in deep or steeply dipping, unminable coal seam. It also lowers the capital investment by eliminating the need for specialised coal processing (transporting and stocking) and gasification reactors. Underground coal gasification (UCG) has other advantages such as increased work safety, no surface disposal of ash, low dust, and noise pollution. It can be operated at high pressure to increase the reaction intensity and improve the efficiency of the process. A comprehensive environmental assessment and risk analysis is required prior to embarking the UCG process because of possibility of land subsidence and ground water pollution, the UCG disadvantages (Lowry, 1963; Perkins, 2005; Khadse et al., 2006).

Several field designs have been operated in order to make UCG functional regarding different operating aspects such as a linking technique, avoiding heat and gas loss into adjacent formation, producing constant high-quality gas, minimising the inhibitor effect of ash, and reducing the environmental effects (Perkins, 2005). Figure 1 illustrates the most applied field designs of the UCG process. Linked vertical wells (LVW) require drilling two vertical wells as the producer and injector and establishing a linking channel between them using various technologies, including hydraulic fracturing, explosive fracture, reverse combustion, and directionally drilling. In the gasification of steeply dipping coal seams, the

*Author to whom correspondence may be addressed.
E-mail address: jabedi@ucalgary.ca
Can. J. Chem. Eng. 89:1528–1535, 2011

DOI 10.1002/cjce.20496
Published online 9 March 2011 in Wiley Online Library (wileyonlinelibrary.com).

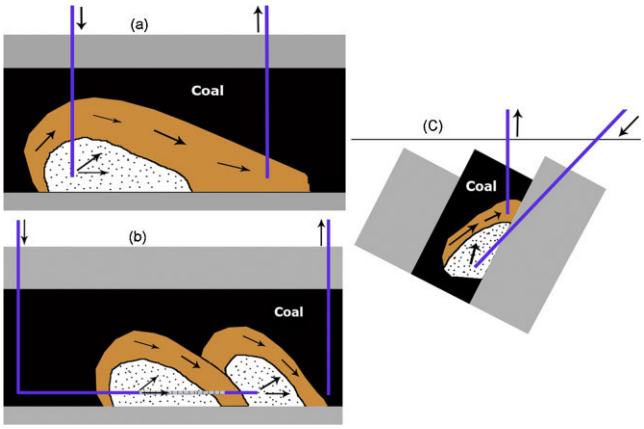

Figure 1. Schematics of most applied field designs of UCG: (a) linked vertical wells, LVW; (b) controlled retracting injection point, CRIP; and (c) steeply dipping coal seams.

injector is drilled at an angle in a lower part of the coal seam and the producer is drilled vertically in an upper part. Also, in order to access fresh coal and minimise the effect of deposited ash dregs over the injection point, a series of injection wells are drilled at an angle over the course of the UCG process. Another technique, the controlled retracting injection point (CRIP) is the most favourable technique of gasification of coal in situ. In the CRIP process, the production well is drilled vertically, and the injector is drilled horizontally close enough to the producer to have considerable flow connection. When the linking channel is established, the coal is ignited at the end of the horizontal well and a cavity is initiated. Once the coal near this cavity is burnt up, the injection point is retracted to a new location to access fresh coal and begin the next cavity. This procedure carries on until the majority of coal between the wells is consumed (Perkins, 2005; Yang, 2005; Burton et al., 2008).

In this work, three-dimensional numerical simulation of the UCG process is studied by using the CRIP technique and a porous media flow approach as in hydrocarbon reservoir simulation. The STARS module of the Computer Modelling Group software (CMG) is used in this study. The major approach is to apply heat and mass transport phenomena in conjunction with chemical reactions in order to investigate the cavity shapes, temperature variation, product gas composition, and flow rates that are the critical aspects of the UCG process.

The modelling of the UCG process has mostly been done by using the computational fluid dynamics (CFD) approach (Shirsat, 1989; Burton et al., 2008). They used complicated velocity equations, included the turbulent gas flow inside a cavity, and utilised chemical engineering correlations for particle sizes, the porosity of a reactor, and an equilibrium controlled formulation for reversible reactions. A porous media approach, which is based on mass conservation, Darcy's law, and energy conservation and accounts for the change in porosity and permeability due to the rock strength change, is more appropriate for the description of UCG. Furthermore, in this approach the reversible reactions are replaced with two irreversible reactions with effective kinetics mechanisms. The focus of this work is to establish this porous media approach for the description of UCG and show that the findings from this approach are in agreement with those in the literature using the CFD approach.

MODEL FORMULATION AND PROPERTIES

Model Structure

The modelling of UCG can generally be divided into two categories: the geomechanic part that deals with cavity shapes, cavity growth mechanisms, subsidence, and other mechanical aspects and the geochemistry part that deals with the fluid flow, product gas composition and calorific value, chemical reactions, and heat and mass transport phenomena. Therefore, the modelling of the UCG process is very complex and involves comprehensive simulation of coupled fluid, chemical, thermal transport, and mechanical deformation processes (Shirsat, 1989). In our model, the cavity growth is caused by char combustion and gasification reactions. Thus, the rate of cavity growth depends on the progress rate of these reactions. Other types of mechanisms such as thermo-mechanical failure, rock spalling, sidewall regression, and bulk collapse of coal need to be included in the future work as a separate module in addition to the STARS module of the CMG software (Britten and Thorsness, 1988).

In this study, a rectangular coal seam with dimensions of 25 m length, 12.5 m width, and 9 m height is used. It is divided into 99 intervals in the x-direction, 49 intervals in the y-direction, and 35 layers in the z-direction numbered downwards. A vertical well located at one extremity of the seam and in the middle of width is considered as the production well. It is extended from the top layer to layer 31 and perforated at the last layer. The injection well is placed horizontally at layer 31 from blocks 2 to 84 in the x-direction and in the same block as the producer in the y-direction. The injector is initially perforated at the toe which is 3 m away from the producer. All boundaries of the seam domain are considered to be no flow. Despite of increasing the runtime of simulation, the grid blocks have been taken to have a very small size ($0.25\,\text{m} \times 0.25\,\text{m} \times 0.25\,\text{m}$) so that the temperature gradient will be more distinguishable and also because STARS uses the average temperature of each block to calculate the chemical reaction constants, having small blocks increases the accuracy of the reaction rates. Figure 2 delineates the structure of the applied coal seam.

Conservation Equations

For investigation of the geochemical behaviour of coal gasification, the momentum balance law for determination of the flow velocity, the mass conservation law for composition prediction, and the energy conservation law for temperature profile prediction are generally considered. In the model, the momentum conservation is approximated by Darcy's law due to the porous media approach used, and all conservation equations are defined in

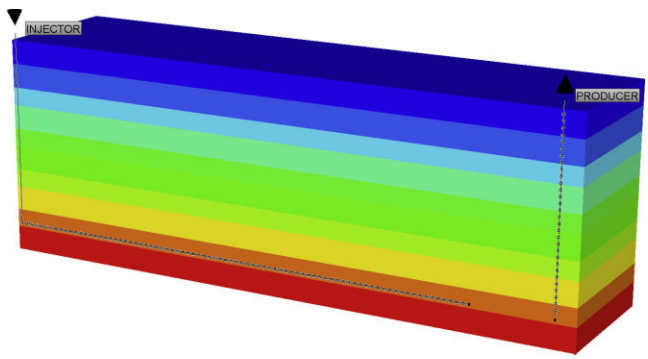

Figure 2. Geological structure of applied coal seam model.

three-dimensional spaces as follows. The radiation effect between incandescent coal surfaces and gas molecules is ignored in heat transport phenomenon.

The momentum balance equation is:

$$v_g = -\frac{k}{\mu_g}\left(\nabla P - \rho_g g \nabla Z\right) \tag{1}$$

The mass balance equation for flowing component i is:

$$\sum_{l=1}^{n_b}\sum_{j=1}^{n_p}\phi D_{ji}\rho_j \Delta y_{ij} + \sum_{l=1}^{n_b}\sum_{j=1}^{n_p} T_j \rho_j y_{ij} \Delta\Phi_j + V\sum_{l=1}^{n_r}(s_{li}' - s_{li})r_l + \sum_{j=1}^{n_p}\rho_j q_{jk} y_{ji} + \delta_{iw}\sum_{l=1}^{n_b}\rho_w q_{aq_{wk}} = \left(\frac{V}{\Delta t}\right)\left(\left(\phi_f\sum_{j=1}^{n_p}(\rho_j S_j y_{ji})\right)^{(n+1)} - \left(\phi_f\sum_{j=1}^{n_p}(\rho_j S_j y_{ji})\right)^{(n)}\right) \tag{2}$$

The first and second expressions are flowing terms, diffusion, and convection, respectively. The mass transfer caused by chemical reactions during the process is illustrated by the third term. The fourth and fifth terms account for the external injection of component i via an injection well or an aquifer influx, respectively. The only term on the right-hand side describes the accumulation of component i in a gird block with the volume of V. The phase j transmissibility, T_j, is defined as:

$$T_j = \left(\frac{A}{\Delta l}\right)\left(\frac{k_j}{\mu_j}\right) \quad j = 1, \ldots, n_p \tag{3}$$

which is a function of the effective permeability, viscosity, cross-sectional area, and node spacing.

The conservation equation of solid component i is:

$$V\sum_{l=1}^{n_r}(s_{li}' - s_{li})r_l = \left(\frac{V}{\Delta t}\right)\left((\phi_v C_i)^{(n+1)} - (\phi_v C_i)^{(n)}\right) \tag{4}$$

Equation (4) describes the variation of concentration of solid component i with time which is only caused by chemical reactions. The left-hand side describes the consumption rate of solid component i during the gasification and the right-hand side is the accumulation term. In our model, two solid components of original coal and char are considered.

The energy conservation equation is:

$$\sum_{l=1}^{n_b}\sum_{j=1}^{n_p} T_j \rho_j H_j \Delta\Phi_j + \sum_{l=1}^{n_b} K\Delta T + V\sum_{l=1}^{n_r} H_{rl} r_l + \sum_{j=1}^{n_p}\rho_j H_j q_{jk}(\text{well}-\text{layer}-k) = \left(\frac{V}{\Delta t}\right)\left(\xi^{(n+1)} - \xi^{(n)}\right) \tag{5}$$

Energy transfer by convection and conduction mechanisms are illustrated by the first and second terms, respectively. The third term accounts for the reaction source/sink term and the last term describes the well source/sink for energy. In the model, neither well term for solid nor heat loss is considered. The accumulation term of energy is included on the right-hand side in which ξ is defined as:

$$\xi = \phi_f\sum_{j=1}^{n_p}\rho_j S_j U_j + \phi_v C_s U_s + (1-\phi_v)U_r \tag{6}$$

Chemical Processes

During in situ combustion of coal different processes of vaporisation (drying), pyrolysis, and combustion and gasification of char take place. Figure 3 illustrates different chemical regions of gasification of coal in situ. In the drying zone, surface water in the wet coal is vaporised at temperatures above the saturation temperature of seam water at a specified pressure, which makes the coal more porous. The dried coal undergoes the pyrolysis process upon more heating in the next phase. During pyrolysis, coal loses about 40–50% of its dry weight as low molecular weight gases, chemical water, light hydrocarbons and heavy tars, and after evolving the volatile matters, a more permeable solid substance called char will be combusted and gasified by the injected oxidant agents and exhausted gases from the previous steps (Campbell, 1976; Merrick, 1983).

The pyrolysis process is a complex thermal decomposition process at the typical temperature range of 400–900°C which results in a series of reactions releasing volatile matters from the porous coal matrix and changes the chemical and physical structure of the coal. Several kinetic models of coal pyrolysis such as the consecutive decomposition, multi-step consecutive-competitive model, simultaneous independent reaction model for each species, and single step decomposition (or overall first-order reaction model) have been proposed in the literature (Tsang, 1980; Perkins, 2005). In this study, the latter model is applied to describe the pyrolysis

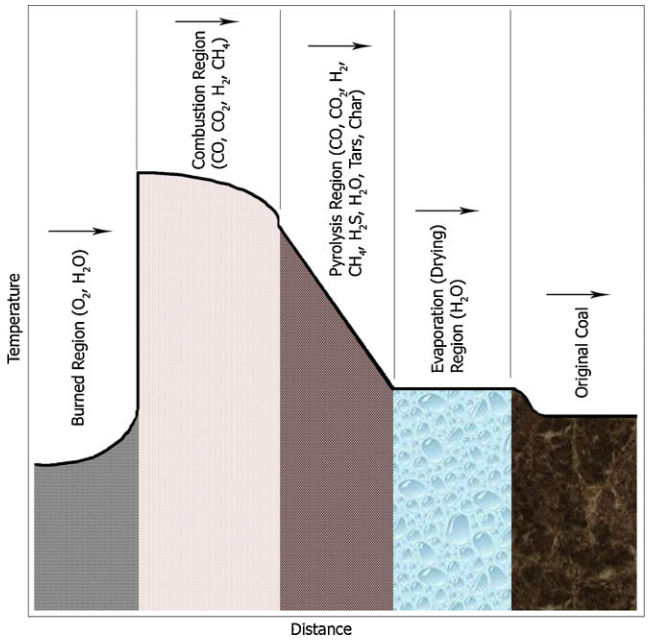

Figure 3. Thermal wave propagation through coal seam during in situ gasification which demonstrates the different regions.

process. It is assumed that the dried coal is decomposed to CO, CO_2, H_2, CH_4, and char as shown in reactions (7) and (8). For simplicity, the char is assumed to be pure carbon. Thus, the effect of ash dreg residuals in the porous medium will be eliminated in this model.

$$\text{Dry}-\text{Coal} \rightarrow \text{Char} + \text{Volatile matter} + \text{Ash} + \text{Chemical water} \quad (7)$$

$$\text{Volatile matter} \rightarrow \alpha_1\text{CO} + \alpha_2\text{CO}_2 + \alpha_3\text{H}_2 + \alpha_4\text{CH}_4 \quad (8)$$

The stoichiometry coefficients have been calculated by using material balance on each element in the reaction and applying the elemental analysis of sub-bituminous coal under study as shown in Table 1. Thus, the final form of the pyrolysis reaction used in the model is:

$$\text{Dry}-\text{Coal} \rightarrow 4.63\ \text{Char} + 0.12\text{CO} + 0.18\text{CO}_2 + 0.43\text{H}_2 + 0.79\text{CH}_4 \quad \Delta\text{H}^0_{298} \approx 0.0 \quad (9)$$

The kinetics of the volatile matter releasing is described during the pyrolysis process in the model by a first-order reaction on the concentration of coal for which the rate varies with temperature according to an Arrhenius relationship below where the values of 1.9e17/day and 180 kJ/mole are used for the pre-exponential factor, κ_0, and activation energy, E, respectively (Merrick, 1983; Vargas and Perimutter, 1985; Ma et al., 1991; Nourozieh et al., 2010)

$$\kappa = \kappa_0 \exp(-E/\text{R}\bar{\text{T}}) \quad (10)$$

A set of heterogeneous reactions between char and gas species mostly on the surface of cavities and homogeneous reactions among gas species inside the cavities take place. The rate of progress of these heterogeneous reactions determines the rate of consumption of carbon and cavity growth, and these homogeneous reactions play the main role in the ultimate composition of the product syngas, particularly the water–gas shift and methane steam reforming reactions. The most important reactions are summarised as follows (Thorsness and Rozsa, 1976; Perkins, 2005; Nourozieh et al., 2010):

$$\text{C} + \text{O}_2 \rightarrow \text{CO}_2 \quad \Delta H^0_{298} = -393\ \text{kJ/mole} \quad (11)$$

$$\text{C} + \text{H}_2\text{O} \rightarrow \text{H}_2 + \text{CO} \quad \Delta H^0_{298} = +131\ \text{kJ/mole} \quad (12)$$

$$\text{C} + \text{CO}_2 \rightarrow 2\text{CO} \quad \Delta H^0_{298} = +172\ \text{kJ/mole} \quad (13)$$

$$\text{C} + 2\text{H}_2 \rightarrow \text{CH}_4 \quad \Delta\text{H}^0_{298} = -75\ \text{kJ/mole} \quad (14)$$

$$\text{CO} + 1/2\text{O}_2 \rightarrow \text{CO}_2 \quad \Delta H^0_{298} = -283\ \text{kJ/mole} \quad (15)$$

$$\text{CO} + \text{H}_2\text{O} \leftrightarrow \text{CO}_2 + \text{H}_2 \quad \Delta H^0_{298} = -41\ \text{kJ/mole} \quad (16)$$

$$\text{CH}_4 + \text{H}_2\text{O} \leftrightarrow \text{CO} + 3\text{H}_2 \quad \Delta H^0_{298} = +206\ \text{kJ/mole} \quad (17)$$

Except reaction (14) which is more effective at high pressures, other reactions are more common for the surface coal gasifiers and shallow UCG processes.

In order to model these reactions that appear as the source/sink terms in the conservation equations, all are treated as first-order reactions based on the concentration of the reactants and using the power law as shown in Equation (18), and the temperature dependent rates are described by the Arrhenius correlation. Reversible reactions are divided into two separate forward and backward reactions when introduced into the STARS simulator. The relevant frequency factors, κ_l, and activation energies, E_l, for these reactions are summarised in Table 2. These are effective kinetic parameters that include the intrinsic kinetics and gas-film diffusion resistance (Nourozieh et al., 2010).

$$r_l = \kappa_l \prod_{i=1}^{n_c} C_i^{\eta_{li}} \quad (18)$$

Model Properties

In the UCG process, the porosity of a block can be divided into two categories: void porosity, ϕ_v, which is defined as the volume fraction of solid and fluid in the block and fluid porosity, ϕ_f, which is the volume fraction of the fluids. Both porosities vary with time as the solid components in the block are consumed. In the model, these parameters are calculated using Equations (19) and (20):

$$\phi_\text{v} = \phi_0\left(1 + C_\text{p}(P - P_\text{r}) - C_\text{T}(T - T_\text{r})\right) \quad (19)$$

$$\phi_\text{f} = \phi_\text{v}\left(1 - \sum_{i=1}^{n_s}(C_{si}/\rho_{si})\right) \quad (20)$$

Permeability is a strong function of the porosity, especially in the case of the UCG process with a high amount of solid consumption; the large change in the void porosity causes a considerable change in the permeability. Large permeability at the same operating conditions makes an easy production of gas species and

Table 1. Coal analysis results

Ultimate analysis	
Moisture	0.89
Ash	9.66
H	3.55
C	73.76
N	1.07
S	0.43
O	10.64
Proximate analysis	
Moisture	4.72
Ash	9.29
Volatile matter	30.46
Fixed carbon	55.54

Table 2. Kinetics parameters of heterogeneous and homogeneous reactions

Reaction no. (l)	Reaction name	E_l (kJ/gmol)	κ_l (1/day)
11	Coal combustion	100	1.80E+06
12	Steam gasification	156	4.70E+07
13	Boudouard	249	6.40E+09
14	Hydrogen gasification	200	1.50E+14
15	Carbon monoxide oxidation	247	6.48E+03
16	Forward water shift	126	2.40E+05
16	Reverse water shift	126	2.40E+03
17	Forward methane steam reforming	30	2.70E+07
17	Reverse methane steam reforming	30	2.70E+08

Table 3. Thermal properties of solids and fluids

Char heat capacity, J/(gmol/°C)	17
Coal heat capacity, J/(gmol/°C)	17
Rock heat capacity, J/(m^3/°C)	3.0E+06
Solid thermal conductivity, J/(m/day/°C)	4.5E+05
Rock thermal conductivity, J/(m/day/°C)	2.0E+05
Water thermal conductivity, J/(m/day/°C)	48,384
Gas thermal conductivity, J/(m/day/°C)	4000

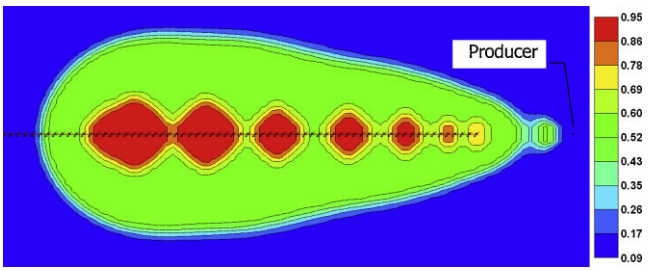

Figure 4. Fluid porosity variation at the end of a 50 days run, *x–y* cross-section.

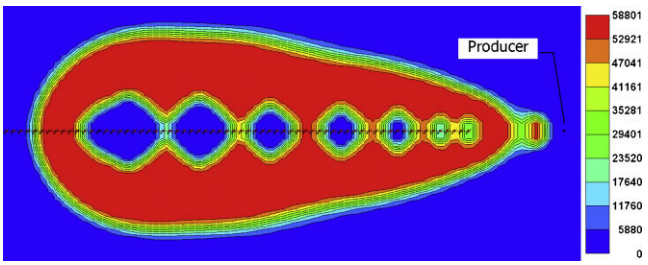

Figure 5. Char concentration variation at the end of 50 days run, *x–y* cross-section.

reduces the contact time for reactions. In this model, the permeability variation is described in exponential form as shown in Equation (21):

$$k = k_0.\exp\left[k_{\text{mul}}\left(\frac{\phi_{\text{f}}-\phi_{\text{f0}}}{1-\phi_{\text{f0}}}\right)\right] \tag{21}$$

Here, k_0 and ϕ_{f0} are the initial permeability and fluid porosity, respectively, and k_{mul} is a multiplier which is taken to be 4 for all directions (Computer Modelling Group, 2009).

Solid and gas heat properties such as heat capacity and thermal conductivity are considered to be constant as shown in Table 3, except the heat capacities of gas species that are calculated by using Equation (22) with the related constant coefficients summarised in Table 4 (Reid et al., 1987, Appendix A; Computer Modelling Group, 2009).

$$Cp_i(T) = \alpha_i + \beta_i T + \gamma_i T^2 + \zeta_i T^3 \tag{22}$$

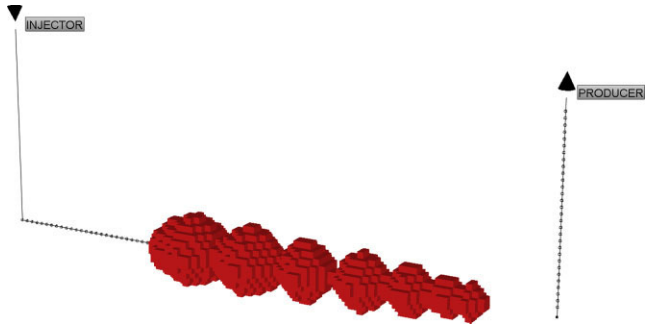

Figure 6. Three-dimensional view of created cavities after 50 days of simulation.

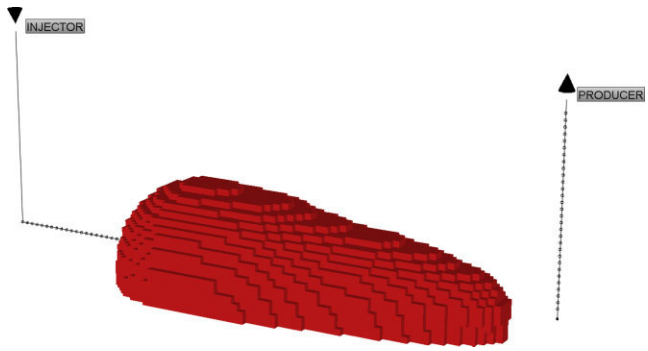

Figure 7. Three-dimensional view of the elliptic form of the whole cavities after 50 days of simulation.

Table 5. Initial properties of the coal seam required for the modelling purpose

Porosity, fraction (coal + initial fluid)	0.95
Absolute permeability, md	1.0
Coal concentration	1.27E+04
Water saturation	0.7
Temperature, °C	60
Pressure, MPa	11.5
Fluid in porous media	CH_4
Coal density, kg/m^3	1200
Char density, kg/m^3	1740

The initial properties of the coal seam required for the modelling purpose are summarised in Table 5. In this model, the equal molar mixture of steam and oxygen is used as oxidant agents. The runtime for this model is about 3 days for 50 days of simulation.

RESULTS AND DISCUSSION

As mentioned earlier, the main goal of this study is to introduce a numerical methodology to simulate the UCG process by using the STARS module of the CMG software in terms of a porous media flow approach. The findings, especially the temperature

Table 4. Values of coefficients for gas species heat capacity correlation

Coefficients	O_2	CO_2	H_2	CO	CH_4
α, J/gmol/C	28.106	19.795	27.14	30.869	19.251
β, J/gmol/C^2	−3.68E−06	7.34E−02	9.27E−03	−1.29E−02	5.21E−02
γ, J/gmol/C^3	1.75E−05	5.60E−05	−1.38E−05	2.79E−05	1.20E−05
ζ, J/gmol/C^4	−1.07E−08	1.72E−08	7.65E−09	−1.27E−08	−1.13E−08

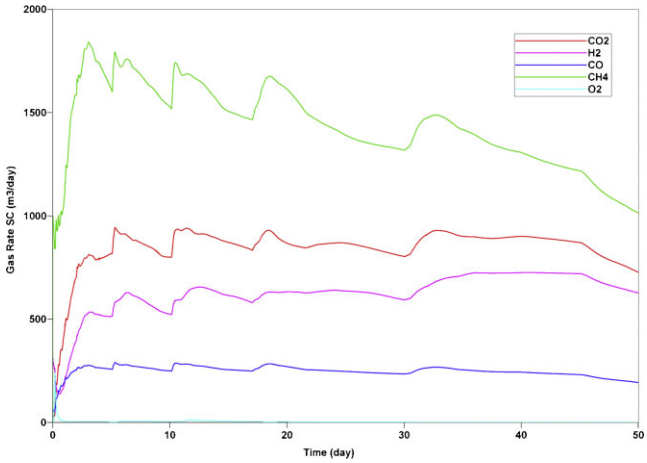

Figure 8. Flow rates of different gas species during 50 days of simulation.

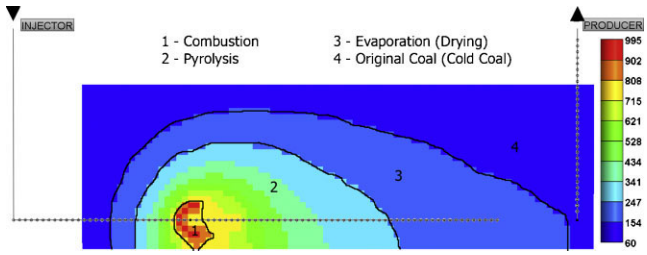

Figure 9. Different chemical regions based on temperature profile.

profile, cavity shape, and compositions of gas species are comparable qualitatively with those reported in the literature. The cavity shape can be investigated by using the values of char/coal concentrations and fluid porosity. Figures 4 and 5 illustrate the profiles of the char concentration and fluid porosity at the end of simulation of 50 days. At the early time of simulation when the injection point is much closer to the perforated interval of the producer, the cavities are smaller and not completely clean from char, because the injection point is retracted after a small time interval in order to prevent the high temperature combustion front to reach the production well. Around each injection point a cavity is developed, and based on the injection time at the same point the size of the cavities is becoming larger as receding from the production well. In the innermost section of each cavity the concentration of the char is 0 and the amount of fluid porosity is the maximum value, only the incombustible solid components remaining; their values are increasing towards the boundaries of the coal seam so that an elliptic shape cavity is generally formed. Having 0 concentration of char outside of the elliptic shape indicates that the pyrolysis front has not reached this section, the original coal remained intact, and the fluid porosity in this part has its lowest value which determines no coal consumption. Figure 6 shows each cavity in the three-dimensional view based on the fluid porosity range of 60–95%. Figure 7 demonstrates the elliptic shape which includes the whole affected volume of the coal seam by the combustion and gasification processes after a 50 days run of simulation.

Figure 8 shows the flow rate of the different gas species during the 50 days run of simulation. As seen, except at the early time which includes the ignition process and generating heat to establish the combustion front, the production rate of all species behaves steady-state and this result conforms to those reported in the literature. Each hump indicates the formation of new cavity in which in addition to access of fresh coal, the intensity of reactions increases due to a lower effect of gas-film resistance and more availability of oxidant agents. The more production of CH_4 at the early time is because of the original existence of the methane in the porous medium, and pyrolysis is the main source of the methane production at the late time. For an appropriately designed gasification reactor, the production of oxygen should be 0 because having a large amount of oxygen production may cause explosion in the producer. In this model, all oxygen is consumed during the gasification.

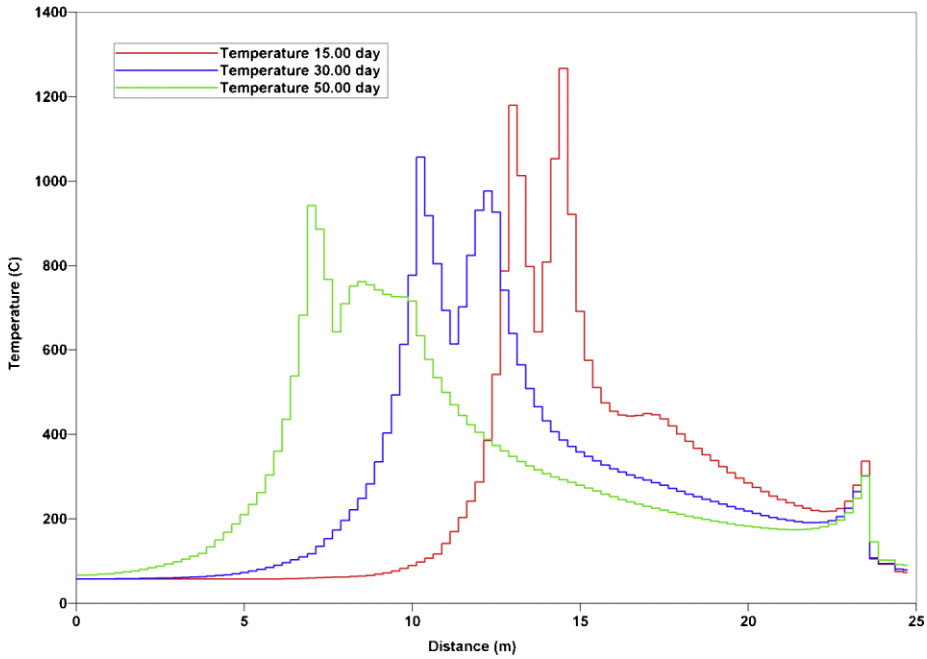

Figure 10. Temperature variation along the length of the coal seam at different times.

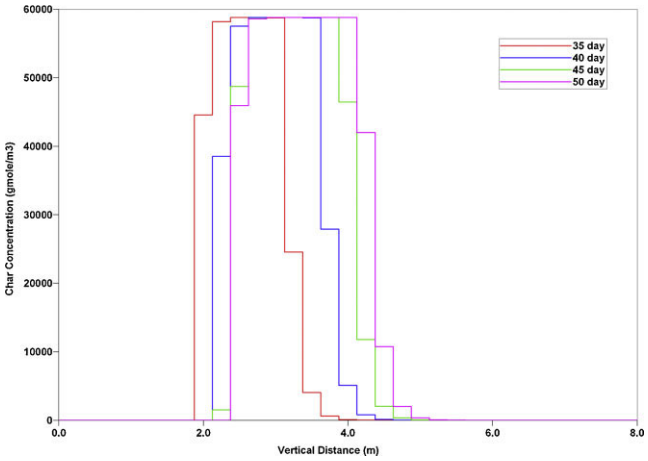

Figure 11. Vertical char concentration profile in the sixth cavity at different times.

The UCG process is composed of three chemical regions of drying, pyrolysis, and combustion and gasification. Figure 9 illustrates these regions qualitatively and quantitatively based on the temperature distribution. As seen, the most inner part with a temperature of around 995°C resembles the combustion front where the main chemical reactions of the UCG process take place. The second region with a temperature range of 250–800°C describes the pyrolysis region. Regions 3 and 4 illustrate the drying and original coal parts, respectively. Figure 10 shows the temperature profile for three different times along the well spacing in layer 31 where the injector is located. The width of plots increases with time, which indicates the increase of gasification length. The maximum temperature decreases with time due to more heat propagation through the coal seam and increasing of the length of the pyrolysis region. Two humps on each plot determine the combustion fronts on both sides of the cavity, which implies that the heterogeneous reactions take place on the sidewall of cavities and there is no spalling of char from the roof of the cavity as expected because the geomechanical mechanisms have not been included in the model.

Figures 11 and 12 depict the typical vertical solid concentration variation profiles at different times during the growth of the sixth cavity. As shown in Figure 11, each char concentration plot begins from the 0 value, indicating the consumption of produced char inside the cavity, and then gradually increases due to the pyrolysis process. It goes through a peak during maximum possible pyrolysis and then declines as the required temperature for pyrolysis decreases. Eventually, it reaches the 0 value wherein, due to the lack of enough heat for pyrolysis, the coal remains unaffected. The width of the char plots increases with time, which indicates that the combustion front (left side of the figure) moves slower than the pyrolysis front (right side of the figure), because heat conduction is faster than the mass transfer and in situ reactions in this process.

Figure 12 confirms the observations of Figure 11. In this figure, each plot begins from the 0 value of the coal concentration in which the coal is completely converted into char and then begins to increase after the corresponding maximum possible char concentration until reaching the initial concentration of coal where there is no char.

CONCLUSIONS

Three-dimensional numerical simulation of the UCG process has been performed by applying the CRIP technique in terms of a porous media flow approach. Despite assuming constant thermal properties for solid components and water and also predicting the pyrolysis process with one reaction, the findings are physically reasonable and in consistent with those in the literature in the light of the syngas flow rate, cavity shape, and temperature profile. Addition of ash as a separate solid whose concentration changes during the gasification may improve the accuracy of the intensity of reactions and results. Including the condensation of steam and tar and also involving N_2, H_2S, C_2H_6, C_3H_8, and C_2H_4 in the released volatile matter during pyrolysis can predict the composition of species more accurately. A geomechanical

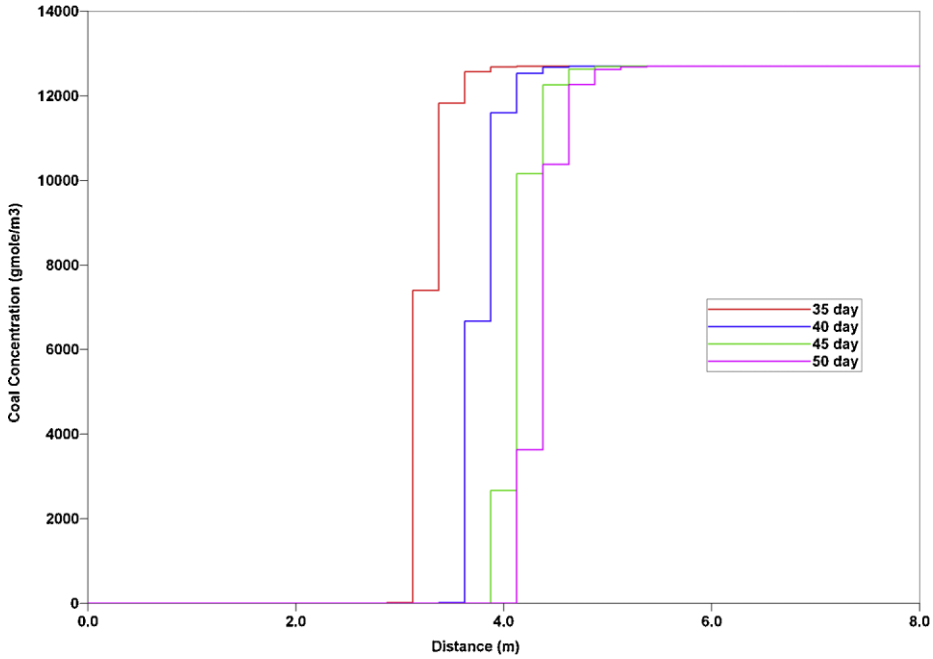

Figure 12. Vertical coal concentration profile in the sixth cavity at different times.

module for UCG, including the modelling of spalling of rock and coal, is being developed by our group. With an appropriate coupling of the model developed in this study and the geomechanical module, the UCG process can more accurately be simulated by using the porous media approach, which will appear in a subsequent article.

NOMENCLATURE

C_i molar concentration of component i, mole/m^3
C_p compressibility, MPa^{-1}
C_r thermal compressibility, $^\circ$C^{-1}
D_{ji} molecular diffusion coefficient of component i in phase j, m^2/s
E activation energy, kJ/mole
G gravity, m/s^2
H_j enthalpy of phase j, kJ/kg
H_{rl} enthalpy of reaction l, kJ/kg
k absolute permeability, md
k_0 initial absolute permeability, md
P fluid phase pressure, MPa
P_r reference pressure, MPa
q_{jk} injection/production flow rate of phase j in layer k of well, m^3/day
r_l rate of reaction l, day^{-1}
s_{li} stoichiometry coefficient of component i in the reactants of reaction l
s'_{li} stoichiometry coefficient of component i in the products of reaction l
s_j saturation of phase j, fraction
T temperature, $^\circ$C
T_j transmissibility term of phase j,$T_j = (A/\Delta l)\left(k_j/\mu_j\right)$
T_r reference temperature, $^\circ$C
U_j internal energy of phase j, kJ/kg
V grid block volume, m^3
y_{ij} mole fraction of component i in phase j, fraction
Z depth, m

Greek Symbols

κ reaction constant, day^{-1}
κ_0 pre-exponential factor (frequency factor), day^{-1}
μ_g gas viscosity, cp
ϕ_f fluid porosity, fraction
ϕ_v void porosity, fraction
ρ_j density of phase j = g, w, solid component, kg/m^3
Φ_j fluid potential, MPa
δ_{iw} mole fraction of component i in aquifer influx, fraction

ACKNOWLEDGEMENTS

This study was supported by the Department of Chemical and Petroleum Engineering at the University of Calgary, Natural Sciences and Engineering Research Council of Canada, Alberta Innovates, and Foundation CMG. Authors also thank Hossein Nourozieh and Mohammad Kariznovi for their constructive comments.

REFERENCES

Britten, J. A. and C. B. Thorsness, "A Mechanistic Model for Axisymmetric Cavity Growth During Underground Coal Gasification," Am. Chem. Soc. **33**, 126–133 (1988).

Burton, E., J. Friedmann and R. Upadhye, "Best Practices in Underground Coal Gasification," Lawrence Livermore National Laboratory, Contract No. W-7405-Eng-48, accessed on: www.purdue.edu/discoverypark/energy/pdfs/cctr/BestPracticesinUCG-draft.pdf Livermore, CA, USA.

Campbell, J. H., "Pyrolysis of Sub-Bituminous Coal As it Relates to In-Situ Gasification (Part 1: Gas Evolution)," University of California, Livermore, CA (1976).

Computer Modelling Group. STARS Technical Manual," Computer Modelling Group LTD., Calgary, Alberta, Canada (2009).

Khadse, A. N., S. M. Mahajani, M. Qayyumi and P. Aghalayam, "Reactor Model for the Underground Coal Gasification (UCG) Channel," Indian Institute of Technology, Bombay (2006).

Lowry, H., "Chemistry of Coal Utilisation," John Wiley and Sons, Inc., New York (1963).

Ma, S., J. O. Hill and S. Heng, "A Kinetic Analysis of the Pyrolysis of Some Australian Coals by Non-Isothermal Thermogravimetry," J. Therm. Anal. **37**, 1161–1177 (1991).

Merrick, D., "Mathematical Models of the Thermal Decomposition of Coal (1. The Evolution of Volatile Matter)," Fuel **62**, 534 (1983).

Nourozieh, H., M. Kariznovi, Z. Chen and J. Abedi, "Simulation Study of Underground Coal Gasification in Alberta Reservoirs: Geological Structure and Process Modelling," Energy Fuels **24**, 3540–3550 (2010).

Perkins, G., "Mathematical modelling of underground coal gasification," PhD Dissertation, The University of New South Wales (2005).

Reid, R. C., J. M. Prausnitz and B. E. Poling, "The Properties of Gases and Liquids," 4th ed., McGraw-Hill, Inc. New York, USA (1987).

Shirsat, V. A., "Modelling of cavity growth in underground coal gasification," MSc. Thesis, Texas Tech University (1989).

Thorsness, C. B. and R. B. Rozsa, "In-situ coal gasification: model calculations and laboratory experiments," SPE Paper, No. 6182, 51st Annual Fall Technical Conference and Exhibition, New Orleans, Oct. 3–6 (1976).

Tsang, T. H. T., "Modelling of heat and mass transfer during coal block gasification," PhD Dissertation, The University of Texas at Austin (1980).

Vargas, J. M. and D. D. Perimutter, "Interpretation of Coal Pyrolysis Kinetics," Ind. Eng. Chem. **25**, 49–54 (1985).

Yang, L. H., "Numerical Study on the Underground Coal Gasification for Inclined Seams," AIChE J. **51**(11), 3059–3071 (2005).

Manuscript received August 10, 2010; revised manuscript received October 4, 2010; accepted for publication October 7, 2010.